EARTHQUAKE ENGINEERING AND STRUCTURAL DYNAMICS
Earthquake Engng Struct. Dyn. 2000; **29**:1629–1646

Seismic structural control using a novel high-performance active mass driver system

Yen-Po Wang*, Chien-Liang Lee and Kwang-Ming Chen

Department of Civil Engineering, National Chiao-Tung University, 1001 Ta Hsueh Road, Hsinchu, Taiwan

SUMMARY

To resolve difficulties encountered by current technology in structural control against earthquakes, this study proposes a novel high-performance active mass driver (HP-AMD) system. Based on an active mass driver system, the device is integrated with a mechanical pulley system for stroke amplification to enhance simultaneously efficiency and save power. Meanwhile, an instantaneous optimal direct output feedback control algorithm is derived alongside the hardware development. Numerical simulation is performed using a five-storey steel frame as the object structure under the 1940 El Centro earthquake. To gain further insight into the HP-AMD system, the effects of stroke amplification as well as damper weight on system performance are explored. Analysis results demonstrate that the proposed HP-AMD system is a promising means to improving current active structural control techniques. Copyright © 2000 John Wiley & Sons, Ltd.

KEY WORDS: seismic structural control; active mass driver system

1. INTRODUCTION

Innovative concepts of structural protection against earthquakes have emerged in recent decades [1, 2]. A new industry integrating aseismic technology production and service has appeared fueled by demand for aftermath reconstruction and retrofit of existing buildings after several devastating earthquakes around the world recently, including the 1999 Ji–Ji earthquake in Taiwan. Modern earthquake protection techniques discard the traditional idea of economy-based design for a performance-based design concept emphasizing maintenance of structural integrity and serviceability even under exceptionally severe earthquakes. Structural control systems that have been implemented include passive, semi-active and active devices. Although active devices have been shown more robust in many aspects than the passive ones, practical concerns such as limited number of sensors and controllers, availability of support utility systems and reliability of a system operates largely in a stand-by mode, have still posed psychological barrier to potential users [3].

* Correspondence to: Yen-Po Wang, Department of Civil Engineering, National Chiao-Tung University, 1000 Ta Hsueh Road, Hsinchu, Taiwan.

Received 15 January 2000
Accepted 31 March 2000

Efficiency enhancement and power saving require hardware development while limited sensing is more of a software problem, which can be dealt with from the control algorithms.

The active devices that have been intensively studied are the active mass damper or active mass driver (AMD) system and the active bracing system (ABS) [4–6]. The AMD can perhaps be implemented better than the ABS as it is structurally less invasive. The active structural systems that have been practically implemented are exclusively of the AMD type which was first applied on a ten-storey office building in Japan for earthquake protection [7, 8]. Herein, this type of control device is considered the basis for further development.

Limited state feedback control can be addressed in three ways: (1) observer and compensator; (2) modal control; and (3) direct output feedback. Since the observer and compensator are themselves electronic dynamic systems, the dimensions of the whole system markedly exceed the measurements of the output. This complexity makes implementation and maintenance difficult. By modal control, physical co-ordinates are converted into modal coordinates and the control law is derived in the reduced-order modal domain. Consequently, spillover induced by the neglected uncontrolled modes of the structure may seriously degrade structural performance. However, the spillover problem vanishes for direct output feedback control since the full-order mathematical model of the structure is considered in the derivation, despite the output measurement containing limited information about the system. Therefore, the direct output feedback strategy suits real implementation. Chung *et al.* [9] developed the optimal direct output feedback control algorithm by minimizing the classical quadratic performance index. Meanwhile, Lin *et al.* [10] further solved the problem of time delay in the context of a direct output feedback control algorithm. Moreover, Chung *et al.* [11] derived an acceleration output feedback control algorithm that was highly practical and allowed an easy and economic measurement of acceleration responses. However, the classical optimal control is not truly optimal because the derivation of the Riccati matrix neglects the excitation [1]. Since at any particular time t, the knowledge of the external excitation may be available up to that time instant t, this knowledge can be utilized to improve control algorithms. Accordingly, Yang *et al.* [12] developed an instantaneous optimal control algorithm by minimizing an instantaneous time-dependent performance index. This algorithm does not require a solution to the Riccati equation, unlike the classical optimal control. The instantaneous control algorithm is modified further in a discrete-time framework with consideration of time delay by Chung *et al*. [13] as is desirable for real-time implementation where digital computers are usually adopted for on-line computation and control execution.

To overcome problems such as insufficient control-force capacity and excessive power demands encountered by current technology in the context of structural control against earthquakes, this study proposes an innovative high-performance active mass driver (HP-AMD) system. This system is based on an active mass driver system comprising of a hydraulic actuator and a mass block, which is integrated with a mechanical pulley system for stroke amplification to achieve efficiency enhancement and power-saving simultaneously. Meanwhile, an instantaneous optimal direct output feedback control algorithm is derived alongside the hardware development to overcome the problem of limited sensing. Numerical simulation is performed using a five-storey steel frame as the object structure under the 1940 El Centro earthquake to investigate the feasibility of the HP-AMD system for earthquake protection of building structures. To improve understanding of the HP-AMD system, the effects of stroke amplification and damper weight on performance are also explored. The analysis results suggest that the proposed HP-AMD system promises to advance the current active structural control techniques.

2. MECHANISM OF THE ACTIVE MASS DRIVER SYSTEM

An active mass driver (AMD) system normally comprises of an actuator (either of hydraulic type or electric type), a servo-control system, a mass block, sensors and a data acquisition system. The design of the HP-AMD system proposed herein is based on the specifications of a 'baby' hydraulic actuator with a maximum dynamic loading of just 1.5 t and a maximum stroke of ± 7.5 cm under a 3000 psi working pressure. This device is specifically designed for seismic control of a five-storey model structure to be tested on a shaking table. To reserve an operative space for the AMD system on the crowded floor plane of $2\,\mathrm{m} \times 2\,\mathrm{m}$ of the model structure, the mass block is elevated and allowed to move on top of the actuator. A preliminary study on an active tuned mass damper (ATMD) system indicates that, constrained by the loading and stroke capacity of the actuator used, the controlling effect of the ATMD system is quite limited. However, system performance can be improved if the mass block is allowed to move in a larger extent. To enhance the performance of the control device, a mechanical pulley system is introduced to extend the stroke of the mass block. This idea then derives the proposed HP-AMD system. The feedback control force applied to the structure is determined in accordance to a certain control law as the next section will explore. Figure 1 illustrates the construction details of the AMD system. The major components of this vibration absorber are further discussed below.

2.1. Hydraulic actuator and connected parts

The HP-AMD system is implemented with an MTS Model 244.11 hydraulic actuator as the mass driver. With an effective piston area of 7.5 cm^2, the actuator provides a maximum loading capacity of 1.5 t, and a maximum stroke of ± 9 cm statistically or ± 7.5 cm dynamically, under a working pressure of 3000 psi. The actuator is installed between a reacting support and a movable steel beam on which a number of movable pulleys are mounted. When activated, the actuator directly drives the movable steel beam which then forces the mass block to move in the opposite direction through the mechanical pulley system, while the reactive force is exerted on the structure for vibration control. The reacting support and the movable steel beam are braced with stiffeners to minimize loss of control force due to deflection. Additionally, a couple of sliding guides in parallel with the actuator are mounted on the front side of the movable steel beam to conduct the sliding motion.

2.2. Mass block

For either an active mass driver system or an active tuned mass damper system, the weight of the mass block significantly affects the system performance and the control force demand. The system is ineffective if the mass block is underweight and impractical if the mass block is overweight. In the proposed system, the mass block is composed of steel plates of various thicknesses to allow for adjustment of the gross weight from 400 kg to 1 t. The mass block is carried by four roller bearings allowed to slide on the rail through a pulley mechanism.

2.3. Mechanical pulley system

The mechanical pulley system is primarily based around twenty pulleys, of which twelve are stationary and eight are movable. According to Figure 1, the stationary pulleys are mounted on two support beams welded near each end of the base plate, whereas the movable pulleys are

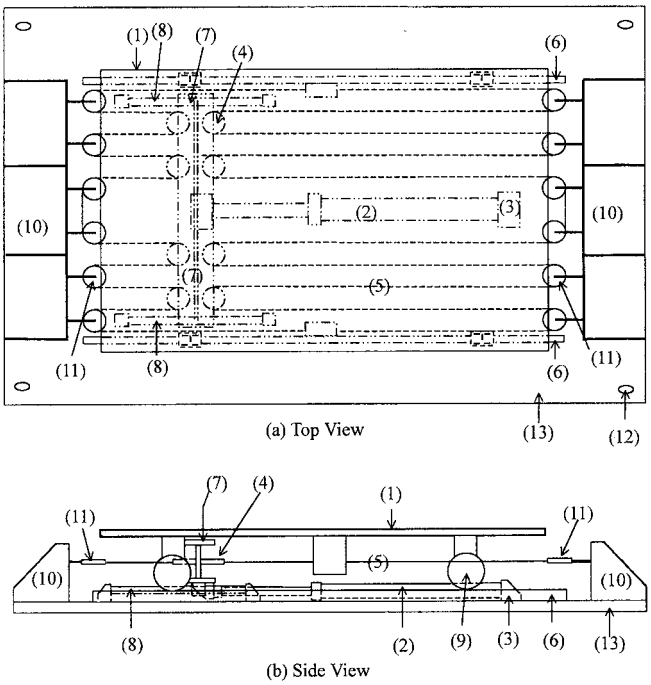

(1) Mass block
(2) Hydraulic actuator
(3) Actuator reacting support
(4) Movable pulley
(5) Pre-stressed tendon
(6) Rail for mass block
(7) Movable steel beam
(8) Sliding guide
(9) Roller
(10) Support beam for stationary pulleys
(11) Stationary pulley
(12) Locking hole
(13) Base plate

Figure 1. Construction detail of the AMD system. (a) Top view; (b) side view: (1) mass block, (2) hydraulic actuator, (3) actuator reacting support, (4) moveable pulley, (5) pre-stressed tendon, (6) rail for mass block, (7) moveable steel beam, (8) sliding guide, (9) roller, (10) support beam for stationary pulleys (11) stationary pulley, (12) locking hole, (13) base plate.

mounted on both sides of the movable steel beam. A prestressed tendon is rove in between the pulleys to form a complete block. With various reeving patterns, as Figures 2(a)–(c) show, denoted respectively with $\alpha = 1, 2$, and 4, the stroke of the mass block can thereby be amplified by α times of the actuator stroke. Meanwhile, the pulley system reduces the force applied to the mass block by α times that driven directly by the actuator. Figure 3 illustrates the motion of the HP-AMD with the pulley block. In the proposed device, the maximum stroke of the mass block can be up to ± 30 cm which corresponds to four times of the maximum available actuator stroke.

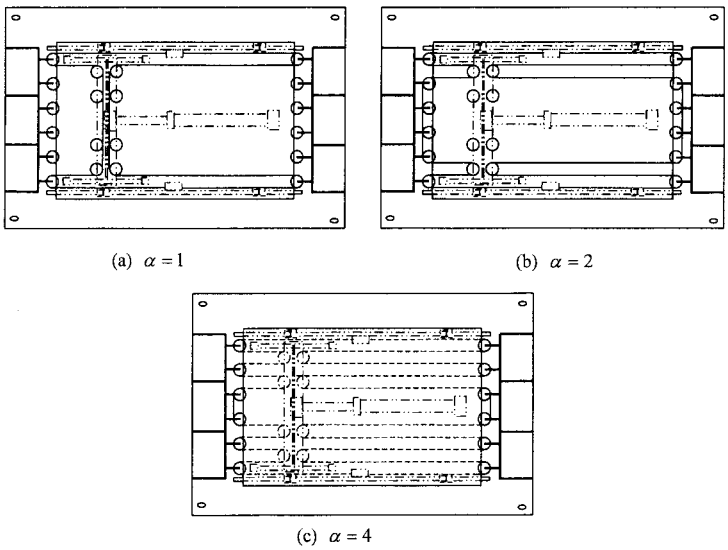

Figure 2. Block reeving patterns of AMD.

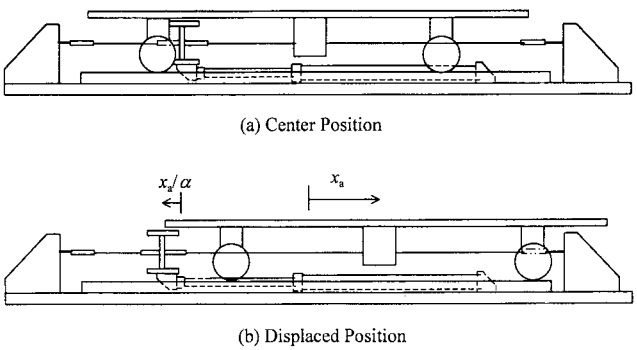

Figure 3. Motion of AMD with pulley block.

3. INSTANTANEOUS OPTIMAL DIRECT OUTPUT FEEDBACK CONTROL

3.1. Discrete-time state-space system

A structural dynamic system, implemented with an active mass driver, subjected to external disturbance $\mathbf{w}(t)$ and control force $\mathbf{u}(t)$ can be described as

$$\mathbf{M}\ddot{\mathbf{x}}(t) + \mathbf{C}\dot{\mathbf{x}}(t) + \mathbf{K}\mathbf{x}(t) = -\mathbf{E}\mathbf{w}(t) + \mathbf{B}\mathbf{u}(t) \tag{1}$$

where $\mathbf{x}$ is the $n \times 1$ displacement vector, $\mathbf{M}$ is the $n \times n$ mass matrix, $\mathbf{C}$ is the $n \times n$ damping matrix, $\mathbf{K}$ is the $n \times n$ stiffness matrix, $\mathbf{w}(t)$ is the $q \times 1$ disturbance vector, $\mathbf{E}$ is the $n \times q$ location matrix of the external disturbances, $\mathbf{u}(t)$ is the $p \times 1$ control force vector and $\mathbf{B}$ is the $n \times p$ location matrix of the control forces.

Equation (1) can be represented in a state-space form, leading to a first-order differential equation as

$$\dot{\mathbf{z}}(t) = \mathbf{A}_c\mathbf{z}(t) + \mathbf{B}_c\mathbf{u}(t) + \mathbf{E}_c\mathbf{w}(t) \tag{2}$$

where

$$\mathbf{Z}(t) = \begin{bmatrix} \mathbf{x}(t) \\ \dot{\mathbf{x}}(t) \end{bmatrix}$$

is the $2n \times 1$ state vector,

$$\mathbf{A}_c = \begin{bmatrix} \mathbf{0} & \mathbf{I} \\ -\mathbf{M}^{-1}\mathbf{K} & -\mathbf{M}^{-1}\mathbf{C} \end{bmatrix}$$

is the $2n \times 2n$ continuous-time system matrix,

$$\mathbf{E}_c = \begin{bmatrix} \mathbf{0} \\ \mathbf{M}^{-1}\mathbf{E} \end{bmatrix}$$

is the $2n \times q$ continuous-time location matrix of the external disturbances, and

$$\mathbf{B}_c = \begin{bmatrix} \mathbf{0} \\ \mathbf{M}^{-1}\mathbf{B} \end{bmatrix}$$

is the $2n \times p$ continuous-time location matrix of the control forces.

If a first-order interpolation of the functions, $\mathbf{u}(\tau)$ and $\mathbf{w}(\tau)$, within any two consecutive sampling points $[k-1, k]$ are considered, then Equation (2) can further be resolved into a recursive discrete-time state equation as

$$\mathbf{Z}[k] = \mathbf{A}\mathbf{Z}[k-1] + (\mathbf{P}_1 + \mathbf{P}_2)(\mathbf{B}_c\mathbf{u}[k] + \mathbf{E}_c\mathbf{w}[k]) - \mathbf{P}_2(\mathbf{B}_c\mathbf{u}[k-1] + \mathbf{E}_c\mathbf{w}[k-1]) \tag{3}$$

where

$$\mathbf{A} = \mathbf{I} + \mathbf{A}_c\varphi\Delta t \tag{4}$$

$$\mathbf{P}_1 = \varphi\Delta t \tag{5}$$

$$\mathbf{P}_2 = \mathbf{\Phi} - \varphi\Delta t \tag{6}$$

$$\varphi = \mathbf{I} + \mathbf{A}_c\mathbf{\Phi} \tag{7}$$

$$\mathbf{\Phi} = \frac{\Delta t}{2}\left[\mathbf{I} + \mathbf{A}_c\frac{\Delta t}{3}\left[\cdots \mathbf{A}_c\frac{\Delta t}{n-1}\left[\mathbf{I} + \mathbf{A}_c\frac{\Delta t}{n}\right]\right]\cdots\right] \tag{8}$$

and $\mathbf{I}$ is a unit matrix. It is noted that, since equation (8) is represented in a nested form, derivation of the discrete-time system matrix, $\mathbf{A}$, and the rest requires no inverse of the continuous-time system matrix, $\mathbf{A}_c^{-1}$. Therefore, they can be obtained without trouble even if matrix $\mathbf{A}_c$ is singular, as is the case of the AMD-controlled structure where the mass driver system contributes no stiffness.

3.2. Direct output feedback control algorithm

Since the transient disturbance function, $\mathbf{w}[k]$, in the discrete-time state Equation (3) cannot be predicted in advance during an episode, this term is therefore neglected in the control design of the active system, and the state Equation (3) is reduced as

$$\mathbf{Z}[k] = \mathbf{B}_1\mathbf{u}[k] + \mathbf{s}[k-1] \tag{9}$$

where

$$\mathbf{s}[k-1] = \mathbf{A}\mathbf{Z}[k-1] - \mathbf{P}_2\mathbf{B}_c\mathbf{u}[k-1] \tag{10}$$

and

$$\mathbf{B}_1 = (\mathbf{P}_1 + \mathbf{P}_2)\mathbf{B}_c \tag{11}$$

Now, if the determination of the optimal feedback control forces is based only on partial output state, $\mathbf{y}[k]$, as

$$\mathbf{u}[k] = \mathbf{G}\mathbf{y}[k] = \mathbf{G}\mathbf{D}\mathbf{Z}[k] \tag{12}$$

where $\mathbf{y}[k]$ is the $r \times 1$ output-state vector ($r \leqslant 2n$), and $\mathbf{D}$ is the $2n \times r$ location matrix of the output state, then it can lead from Equations (9), (10) and (12) to

$$\mathbf{Z}[k] = (\mathbf{I} - \mathbf{B}_1\mathbf{G}\mathbf{D})^{-1}\mathbf{s}[k-1] \tag{13}$$

Define the instantaneous performance index, $J[k]$, for any time instant k as

$$J[k] = \mathbf{Z}^{\mathrm{T}}[k]\mathbf{Q}\mathbf{Z}[k] + \mathbf{u}^{\mathrm{T}}[k]\mathbf{R}\mathbf{u}[k] \tag{14}$$

where the weighting matrices $\mathbf{Q}$ and $\mathbf{R}$ are, respectively, semi-positive definite and positive definite so that an optimal solution exists. In this paper, the weighting matrix

$$\mathbf{Q} = \begin{bmatrix} \mathbf{K} & \mathbf{0} \\ \mathbf{0} & \mathbf{M} \end{bmatrix}$$

is adopted to reserve meaningful physical interpretations of the first term on the right-hand side (RHS) of Equation (14) as the sum of strain energy and kinetic energy of the vibrating structure. Moreover, $\mathbf{R}$ reduces to a scalar if only a single-AMD system is to be implemented.

Substitution of Equations (12) and (13) into Equation (14) leads to

$$J[k] = \mathbf{s}^{\mathrm{T}}[k-1]\mathbf{H}\mathbf{s}[k-1] \tag{15}$$

where

$$\mathbf{H} = (\mathbf{I} - \mathbf{B}_1\mathbf{G}\mathbf{D})^{-\mathrm{T}}(\mathbf{Q} + \mathbf{D}^{\mathrm{T}}\mathbf{G}^{\mathrm{T}}\mathbf{R}\mathbf{G}\mathbf{D})(\mathbf{I} - \mathbf{B}_1\mathbf{G}\mathbf{D})^{-1} \tag{16}$$

It is noted that $J[k] \geqslant 0$ since energy is non-negative. If $\eta_1, \eta_2, \eta_3, \ldots, \eta_{2n}$ are the eigenvalues of matrix $\mathbf{H}$, then J is minimum as $\eta_1 + \eta_2 + \eta_3 + \cdots + \eta_{2n}$ is minimum, for $J[k] \geqslant 0$. That is,

$$\frac{\mathrm{d}J}{\mathrm{d}\mathbf{G}} = \frac{\mathrm{d}(\eta_1 + \eta_2 + \eta_3 + \cdots + \eta_{2n})}{\mathrm{d}\mathbf{G}} = \frac{\mathrm{d}\mathrm{tr}(\mathbf{H})}{\mathrm{d}\mathbf{G}} = \mathbf{0}_{p\times 2n} \tag{17}$$

The feedback gain matrix, $\mathbf{G}$, can hence be resolved from Equation (17) as

$$\mathbf{G} = -\mathbf{R}^{-1}\mathbf{B}_1^{\mathrm{T}}(\mathbf{I}-\mathbf{B}_1\mathbf{G}\mathbf{D})^{-\mathrm{T}}(\mathbf{Q}+\mathbf{D}^{\mathrm{T}}\mathbf{G}^{\mathrm{T}}\mathbf{R}\mathbf{G}\mathbf{D})(\mathbf{I}-\mathbf{B}_1\mathbf{G}\mathbf{D})^{-1}(\mathbf{I}-\mathbf{B}_1\mathbf{G}\mathbf{D})^{-\mathrm{T}}\mathbf{D}^{\mathrm{T}} \times[\mathbf{D}(\mathbf{I}-\mathbf{B}_1\mathbf{G}\mathbf{D})^{-1}(\mathbf{I}-\mathbf{B}_1\mathbf{G}\mathbf{D})^{-\mathrm{T}}\mathbf{D}^{\mathrm{T}}]^{-1} \tag{18}$$

3.3. Numerical solution for the feedback gain matrix [11]

Note that the gain matrix $\mathbf{G}$ in Equation (18) is not expressed explicitly. It can be obtained numerically based on an iterative procedure as follows:

(1) $i=1$.
(2) Let $\mathbf{G}^{(i)}=\mathbf{0}$.
(3) $\bar{\mathbf{G}}^{(i)}=-\mathbf{R}^{-1}\mathbf{B}_1^{\mathrm{T}}(\mathbf{I}-\mathbf{B}_1\mathbf{G}^{(i)}\mathbf{D})^{-\mathrm{T}}(\mathbf{Q}+\mathbf{D}^{\mathrm{T}}\mathbf{G}^{(i)^{\mathrm{T}}}\mathbf{R}\mathbf{G}^{(i)}\mathbf{D})(\mathbf{I}-\mathbf{B}_1\mathbf{G}^{(i)}\mathbf{D})^{-1}(\mathbf{I}-\mathbf{B}_1\mathbf{G}^{(i)}\mathbf{D})^{-\mathrm{T}}\mathbf{D}^{\mathrm{T}}[\mathbf{D}(\mathbf{I}-\mathbf{B}_1\mathbf{G}^{(i)}\mathbf{D})^{-1}(\mathbf{I}-\mathbf{B}_1\mathbf{G}^{(i)}\mathbf{D})^{-\mathrm{T}}\mathbf{D}^{\mathrm{T}}]^{-1}$.
(4) $\mathbf{G}^{(i+1)}=(\mathbf{G}^{(i)}+\lambda\bar{\mathbf{G}}^{(i)})/(1+\lambda)$ (λ is a progressive step factor. The smaller the factor, the slower the rate of convergence, but the better the stability).
(5) Stop iteration if $|\mathbf{G}^{(i+1)}-\mathbf{G}^{(i)}|\leqslant\varepsilon$ where ε is the tolerance of error.
(6) $i=i+1$, go to step (3).

4. NUMERICAL EXAMPLE

4.1. System modeling and performance assessment

As the proposed HP-AMD system is to be placed on the roof of the five-storey model structure for seismic response control, parameters in system equation (1) can further be expressed as

$$\mathbf{x}=\begin{bmatrix} x_a \\ \mathbf{x}_s \end{bmatrix}$$

is the 6×1 displacement vector, where x_a is the displacement of the mass block (relative to ground), and $\mathbf{x}_s$ is the displacement vector of the structure (relative to ground);

$$\mathbf{M}=\begin{bmatrix} m_a & \mathbf{0} \\ \mathbf{0} & \mathbf{M}_s \end{bmatrix}$$

is the 6×6 mass matrix, where $\mathbf{M}_s$ is the mass matrix of the structure, and m_a is the mass of the mass block;

$$\mathbf{C}=\begin{bmatrix} \mathbf{C}_a & -\mathbf{C}_a\mathbf{L}^{\mathrm{T}} \\ -\mathbf{C}_a\mathbf{L} & \mathbf{C}_s+\mathbf{L}C_a\mathbf{L}^{\mathrm{T}} \end{bmatrix}$$

is the 6×6 damping matrix, where $\mathbf{C}_s$ is the damping matrix of the structure, C_a is the damping of the AMD system ($\mathbf{C}_a=0$ in the present case), and $\mathbf{L}=[1\ 0\ 0\ 0\ 0]^{\mathrm{T}}$;

$$\mathbf{K}=\begin{bmatrix} \mathbf{K}_a & -\mathbf{K}_a\mathbf{L}^{\mathrm{T}} \\ -\mathbf{K}_a\mathbf{L} & \mathbf{K}_s+\mathbf{L}\mathbf{K}_a\mathbf{L}^{\mathrm{T}} \end{bmatrix}$$

Table I. System parameters of the five storey model structure.

Mode	1	2	3	4	5
Frequency (Hz)	2.77	9.75	17.82	20.55	27.02
Damping ratio (%)	0.35	0.73	1.80	5.0	5.0
Mode shapes					
5f	0.574	−0.583	0.517	−0.244	0.154
4f	0.561	−0.160	−0.425	0.544	−0.423
3f	0.481	0.347	−0.457	−0.300	0.588
2f	0.324	0.589	0.303	−0.363	−0.566
1f	0.141	0.408	0.501	0.650	0.364
System matrices					
Mass matrix (kg s^2/m)	82.02	0	0	0	0
	0	84.32	0	0	0
	0	0	84.32	0	0
	0	0	0	84.32	0
	0	0	0	0	84.68
Stiffness matrix (kg/m)	513553.3	−525459	12804.06	−24463.4	112196
	−525459	1059683	−637327	141584.6	−121829
	12804.06	−637327	1231284	−733543	49065.2
	−24463.4	141584.6	−733543	1174386	−594433
	112196	−121829	49065.2	−594433	1247133
Damping matrix (kg s/m)	207.53	−293.99	112.21	1.1	−20.68
	−293.99	645.65	−468.21	78.35	88.75
	112.21	−468.21	674.68	−387.97	27.05
	1.1	78.35	−387.97	660.46	−482.53
	−20.68	88.75	27.05	−482.53	754.89

is the 6×6 stiffness matrix, where $\mathbf{K}_s$ is the stiffness matrix of the structure, and $\mathbf{K}_a$ is the stiffness of the AMD system ($\mathbf{K}_a = 0$ in the present case);

$$\mathbf{E} = \begin{bmatrix} -m_a \\ -\mathbf{M}_s\mathbf{1} \end{bmatrix}$$

is the 6×1 location matrix of the earthquake where $\mathbf{1} = [1\ 1\ 1\ 1\ 1]^{\mathrm{T}}$; and

$$\mathbf{B} = \begin{bmatrix} -1/\alpha \\ \mathbf{L} \end{bmatrix}$$

is the 6×1 location matrix of the control force, where α is the amplification factor of the AMD stroke.

System parameters of the model structure are summarized in Table I.

Moreover, from Equations (3) and (13), the discrete-time state-space equation can be further written as

$$\mathbf{Z}[k] = \mathbf{A}_{\mathrm{u}}\mathbf{Z}[k-1] + \mathbf{E}_1\mathbf{w}[k] + \mathbf{E}_0\mathbf{w}[k-1] \tag{19}$$

in which

$$\mathbf{A}_{\mathrm{u}} = (\mathbf{I} - \mathbf{B}_1\mathbf{G}\mathbf{D})^{-1}(\mathbf{A} - \mathbf{P}_2\mathbf{B}_{\mathrm{c}}\mathbf{G}\mathbf{D}) \tag{20}$$

$$\mathbf{E}_1 = (\mathbf{I} - \mathbf{B}_1\mathbf{G}\mathbf{D})^{-1}(\mathbf{P}_1 + \mathbf{P}_2)\mathbf{E}_c \tag{21}$$

$$\mathbf{E}_0 = -(\mathbf{I} - \mathbf{B}_1\mathbf{G}\mathbf{D})^{-1}\mathbf{P}_2\mathbf{E}_c \tag{22}$$

Equation (19) is the basis for assessment the performance of the active structural control system. Through eigenvalue analysis of the effective system matrix, $\mathbf{A}_u$, the equivalent model frequencies and damping factors of the system can be evaluated. Whether or not the control design is sufficient can be ascertained by comparing the dynamic characteristics extracted.

This section first investigates the feasibility of direct output feedback considering moderate measurements. Analysis results are then compared with those from its state feedback counterpart. Moreover, extensive parametric studies are conducted. Also discussed herein are the effects of the stroke amplification factor α and damper weight on the control efficacy of the HP-AMD system.

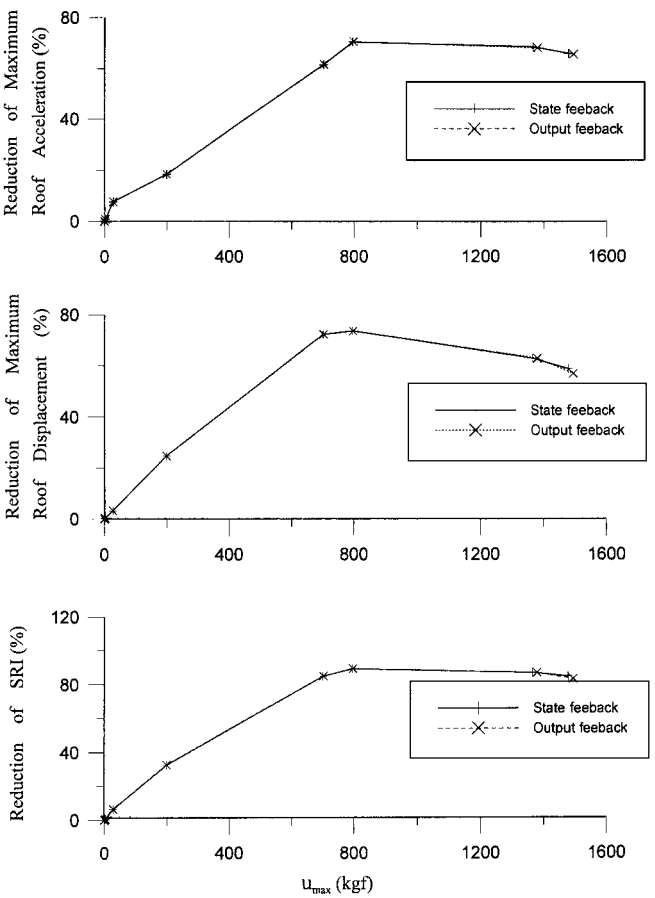

Figure 4. Efficiency curves of control—output feedback vs. state feedback ($m_a = 400$ kg, $\alpha = 4$).

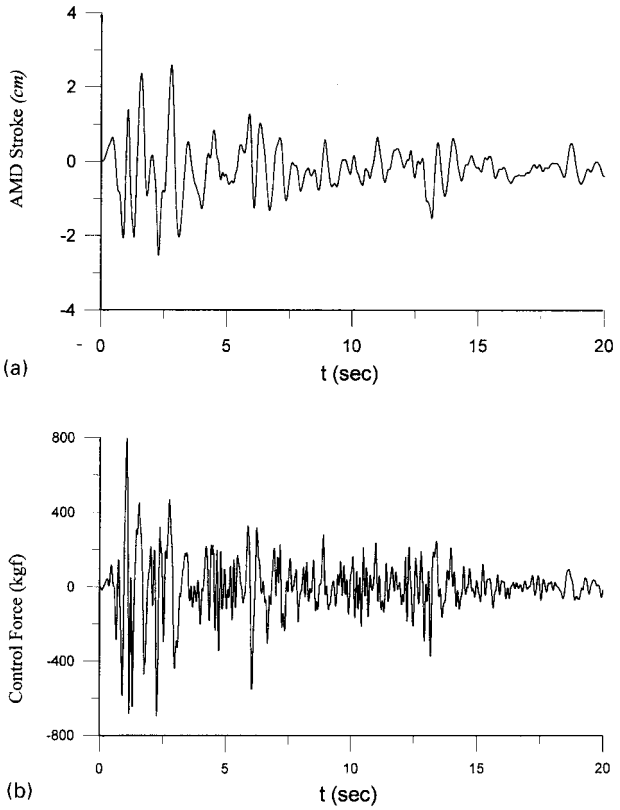

Figure 5. (a) AMD stroke ($m_a = 400$ kg, $\alpha = 4$, $R = 6 \times 10^{-7}$); (b) control force from actuator ($m_a = 400$ kg, $\alpha = 4$, $R = 6 \times 10^{-7}$).

4.2. Verification of direct output feedback control algorithm

A direct output feedback control algorithm achieves an optimal control goal with only moderate response measurements of the structure. Although direct output of a structure generally includes displacement, velocity, and acceleration of any floor, velocity feedback is shown to be sufficient and the most effective [9]. Besides, velocity measurement is easier to implement than displacement measurement, which inevitably requires a rigid frame as reference. Therefore, the present study only considers the top floor velocity ($\dot{x}_5$) and the AMD velocity ($\dot{x}_a$) as the output feedback states for structural control. This example sets the weight of the mass block of 400 kg about 10 per cent of the weight of the structure), designs the system with a stroke amplification factor $\alpha = 4$ as in Figure 2(c), and uses the 1940 El Centro earthquake (N–S) as the input disturbance. Control efficiency is assessed by investigating top floor acceleration, top floor displacement and the overall structural response index (SRI), which is defined as the sum of the strain energy and the kinetic energy of the structure during the entire earthquake.

Figure 4 illustrates the efficiency curves of control in terms of reductions of maximum roof acceleration, maximum roof displacement, and structural response index (SRI), with respect to the

Table II. Eigenvalue analysis—effects of stroke amplification ($m_a = 400$ kg).

Mode	Frequency (Hz)	Damping (%)	Mode	Frequency (Hz)	Damping (%)
	Without control			$\alpha = 2,\ R = 10^{-6}$	
1	2.77	0.35	1	2.18	9.14
2	9.75	0.73	2	8.81	12.80
3	17.82	1.80	3	17.22	9.62
4	20.55	5.00	4	20.33	6.00
5	27.02	5.00	5	27.00	5.58
	$\alpha = 1,\ R = 10^{-5}$			$\alpha = 4,\ R = 6 \times 10^{-7}$	
1	2.69	4.19	1	1.49	27.55
2	9.72	2.47	2	7.91	21.34
3	17.83	2.68	3	16.37	13.46
4	20.55	5.18	4	20.21	5.83
5	27.03	5.06	5	26.93	5.85

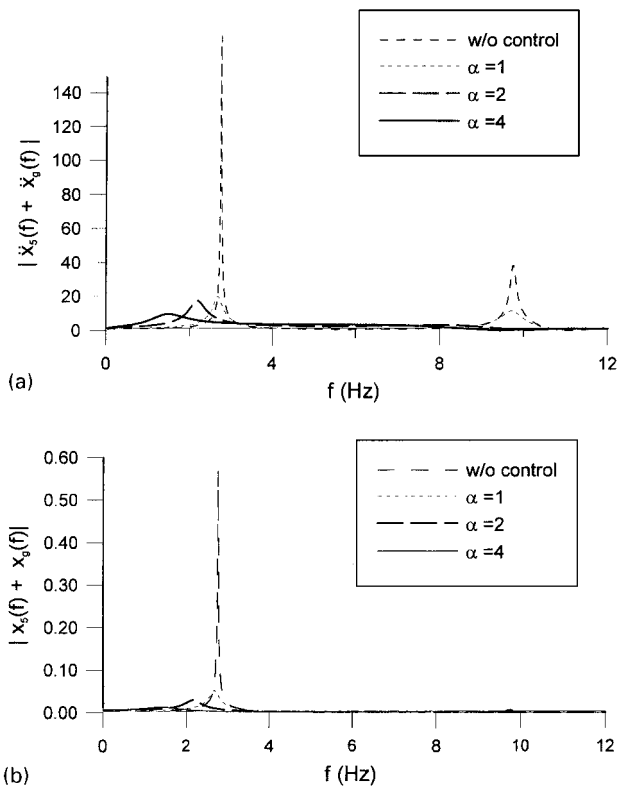

Figure 6. Transfer function of top floor acceleration ($m_a = 400$ kg).

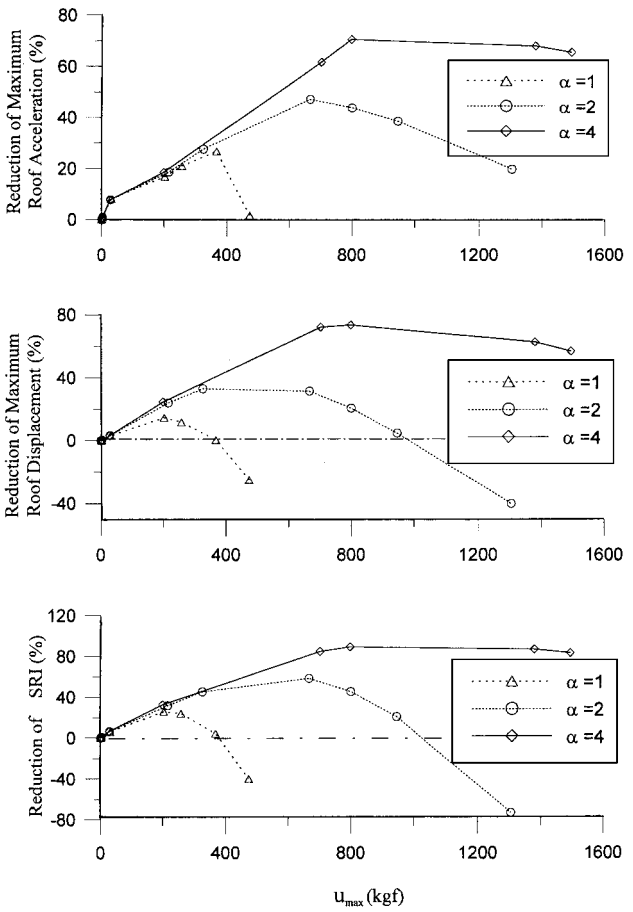

Figure 7. Efficiency curves of control—effects of stroke amplification ($m_a = 400$ kg).

maximum control force, $u_{\max}$, demanded by the control system with $m_a = 400$ kg and $\alpha = 4$. The control efficiency increases with the applied control force until $u_{\max} \approx 800$ kg, which is around twice the weight of the damper. Note that the maximum control force increases as the weighting factor R decreases. The best case, with $R = 6 \times 10^{-7}$, achieves peak reductions with roof acceleration reduced by 70 per cent, roof displacement by 73 per cent, and SRI by 89 per cent. Figures 5(a) and 5(b) illustrate the time histories of the AMD stroke and the control force, respectively. The maximum stroke is 2.59 cm for the AMD (0.65 cm for the actuator correspondingly), which is considerably smaller than what would be expected for an ATMD system.

Furthermore, the efficiency curves of control corresponding to the direct output feedback control and the state feedback control are almost identical. This phenomenon indicates that the proposed direct output feedback control with measurements of only the velocities of the roof and the AMD is functionally equivalent to the state feedback control. The algorithm is therefore highly effective for actual implementation as it requires considerably less measurements than alternatives.

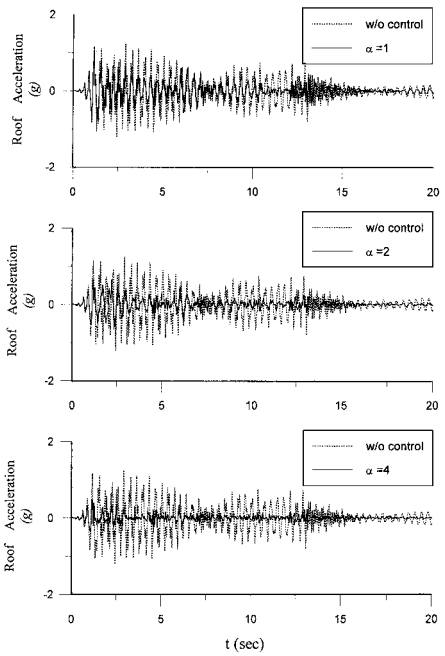

Figure 8. Roof acceleration response history ($m_a = 400$ kg).

4.3. *Effect of AMD stroke amplification on system performance*

This section investigates the effect of AMD stroke amplification on system performance. Considered herein are the block reeving patterns of the AMD system with amplification factor $\alpha = 1, 2$ and 4, as illustrated in Figures 2(a), (b) and (c), respectively. The weight of the mass block is maintained at 400 kg as in the previous example.

Dynamic characteristics of the structure implemented with the AMD system of different reeving patterns are first explored via eigenvalue analysis. As Table II shows, the frequency of the first two modes tend to be lower when AMD is implemented. Moreover, the larger the α, the further left the frequency is shifted. Additionally, the equivalent modal damping ratios increase with α. Taking the case with $\alpha = 4$ for instance, the damping ratio of the first mode increases from 0.35 to 27.55 per cent, from 0.73 to 21.34 per cent for the second mode, and from 1.80 to 13.46 per cent for the third mode. These increases indicate the AMD system greatly improves the dynamic characteristics of the structure. The effectiveness of AMD is also revealed from the frequency response functions of the top floor acceleration (Figure 6(a)) and from the top floor displacement (Figure 6(b)) where the peaks are reduced significantly. Moreover, the efficiency curves of control obtained under the El Centro earthquake (Figure 7) also indicate that the system performs better and better utilizes the capacity of the actuator as the stroke amplification factor α is increased. The maximum control force, $u_{\max}$, required to optimally control the systems with $\alpha = 1, 2$ and 4 is 200, 670 and 800 kg. Finally, the top-floor acceleration history (Figure 8) and the top floor displacement history (Figure 9) show that the extent of response reduction is enhanced clearly when α is increased.

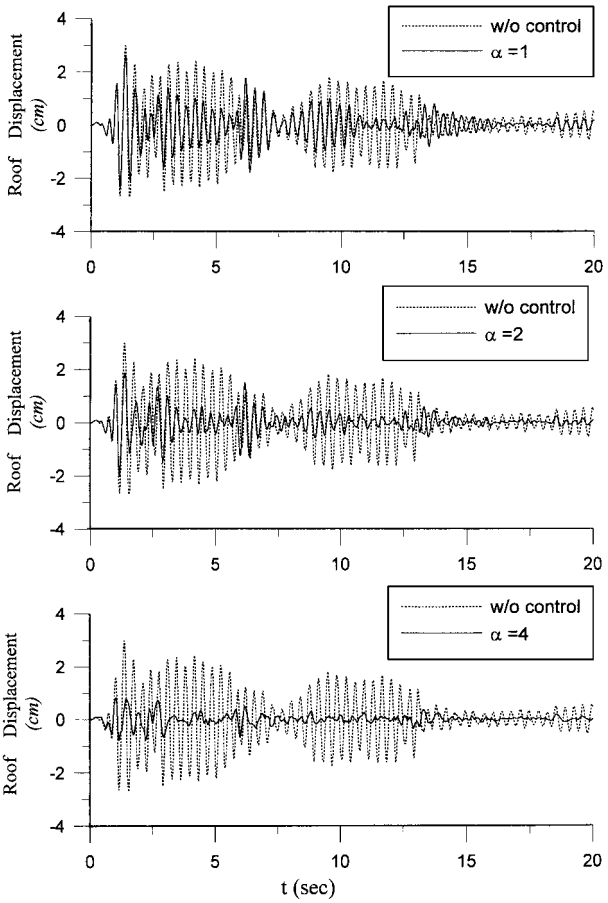

Figure 9. Roof displacement response history ($m_a = 400$ kg).

The maximum power required by the hydraulic system for control execution can be estimated by $\max |u(t)[\dot{x}_a(t) - \dot{x}_5(t)]/\alpha|$. For systems with various stroke amplification factors ($\alpha = 1, 2, 4$), Figure 10 shows the time histories of the power demands under the 1940 El Centro earthquake. For $\alpha = 1$ (i.e. without stroke amplification) with $R = 10^{-5}$ – the optimum design in this configuration is determined from Figure 7, and has the maximum power demand of 799 W which achieves approximately 20 per cent reduction in SRI. For $\alpha = 2$ with $R = 10^{-6}$, the maximum power demand is slightly increased to 808 W and performance significantly improves with approximately a 60 per cent reduction in SRI. For $\alpha = 4$ with $R = 6 \times 10^{-7}$, the maximum power demand is cut drastically to 410 W while it greatly enhances control effectiveness by achieving an 89 per cent reduction in SRI. The AMD system with a pulley mechanism for stroke amplification is not only effective but also efficient.

4.4. Effect of damper weight on system performance

This section further examines the effect of damper weight on system performance. This example sets the weight of the mass block, m_a, as 100, 400 and 800 kg which, respectively, correspond to

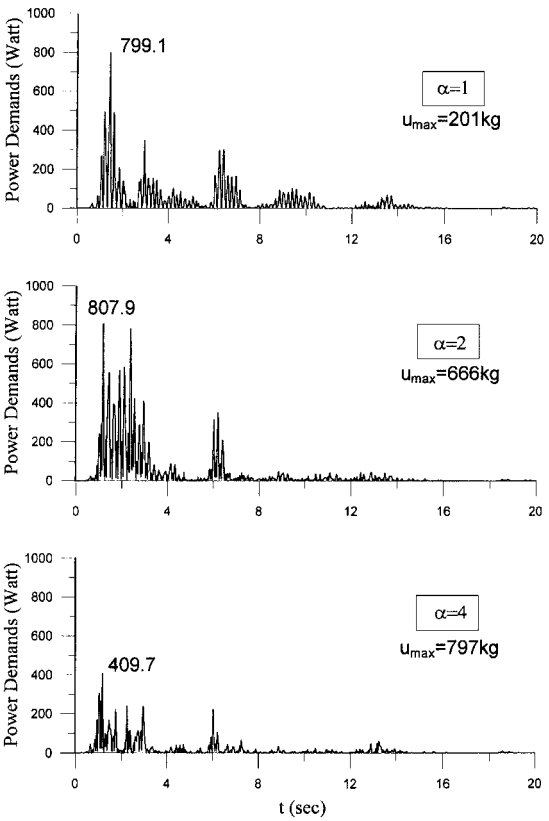

Figure 10. Power demands from actuator ($m_a = 400$ kg).

2.5, 10 and 20 per cent of the weight of the structure, while the stroke amplification factor is set at $\alpha = 4$. The efficiency curves (Figure 11) indicate that substantial improvements can be achieved as m_a increases from 100 to 400 kg. However, the improvement is limited as m_a increases from 400 to 800 kg. Thus, it appears, at least for this particular structure, that the control efficiency of the AMD approaches saturation when the damper weight is 10 per cent of the weight of the structure.

5. CONCLUSIONS

This study proposes a high-performance active mass driver system for earthquake protection of building structures. The system integrates a hydraulic actuator with a mechanical pulley system, amplifying the AMD stroke to permit an effective control without excessive hydraulic power. An instantaneous optimal direct output feedback control law is derived alongside the hardware development. Feasibility of the proposed system is verified through numerical simulations of a five-storey model structure. The HP-AMD system is sufficiently effective using only the velocity measurements of the top floor and the damper. The effects of stroke amplification factor and damper

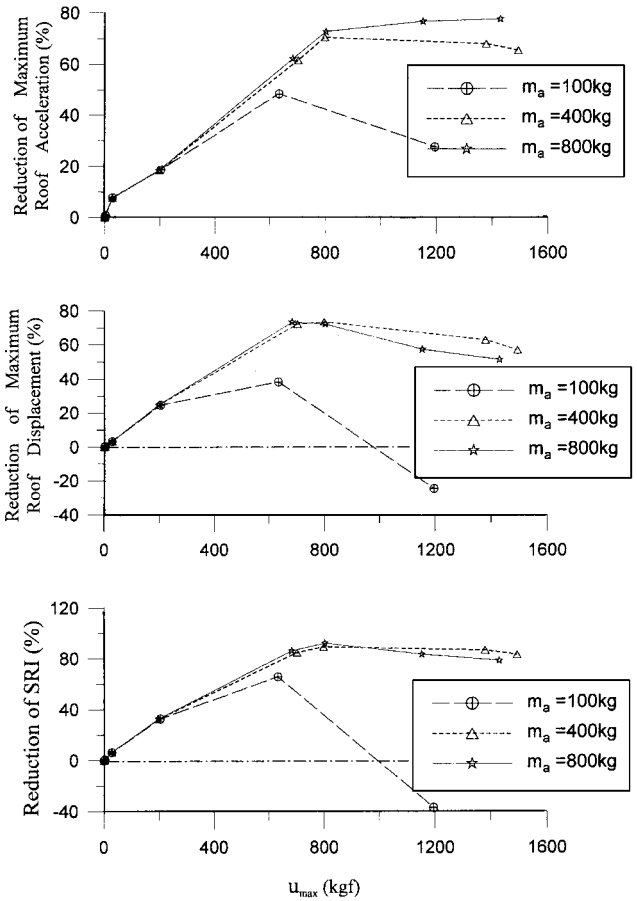

Figure 11. Efficiency curves of control—effects of damper weight ($\alpha = 4$).

weight on system performance have been explored. In accordance with the simulation results, the conclusions are summarized as:

(1) The HP-AMD system is shown effective for seismic structural control. Reduction of the peak responses can reach 70 per cent if properly designed.
(2) The direct output feedback control with moderate measurements is functionally equivalent to the state feedback control.
(3) The AMD system with a pulley mechanism for stroke amplification is not only effective, but also power efficient.
(4) Larger stroke amplification factor improves control efficiency.
(5) Larger stroke amplification factor increases utilization of the actuator capacity.
(6) A greater damper weight improves the control effect. However, the control efficiency of the system appears to reach saturation as the damper weight approaches 10 per cent of the weight of the structure.

ACKNOWLEDGEMENTS

The authors would like to thank Dr L. L. Chung, National Centre for Research on Earthquake Engineering, Taiwan, R.O.C., for his valuable discussions. The authors would also like to thank the National Science Council of the Republic of China for financially supporting this research under Grant No. NSC 88-2625-Z-009-001.

REFERENCES

1. Soong TT. State-of-the-art-review: active structural control on civil engineering. *Engineering Structures* 1988; **10**: 74–84.
2. Soong TT, Masri SF, Housner GW. An overview of active structural control under seismic loads. *Earthquake Spectra* 1991; **7**(3): 483–505.
3. Kobori T. Future direction on research and development of seismic-response-controlled structure. *Proceedings of the First World Conference on Structural Control* 1994; 19–31.
4. Reinhorn AM, Soong TT, Lin RC, Riley MA, Wang YP, Aizawa S, Higashino M. Active bracing system: a full scale implementation of active control. *Technical Report*, *NCEER-92-0020*, NCEER/SUNY/Buffalo, 1992.
5. Reinhorn AM, Soong TT, Lin RC, Wang YP, Fukao Y, Abe H, Nakai M. 1:4 scaled model studies of active tendon systems and active mass dampers for aseismic protection. *Technical Report*, *NCEER-89-0026*, NCEER/SUNY/Buffalo, 1989.
6. Soong TT. *Active Structural Control: Theory and Practice*. Wiley: New York, 1990.
7. Kobori T, Koshika N, Yamada K, Ikeda Y. Seismic-response-controlled structure with active mass driver system. Part 1: design. *Earthquake Engineering and Structural Dynamics*, 1991; **20**: 133–149.
8. Kobori T, Koshika N, Yamada K, Ikeda Y. Seismic-response-controlled structure with active mass driver system. Part 2: verification. *Earthquake Engineering and Structural Dynamics*, 1991; **20**: 151–166.
9. Chung LL, Lin CC, Chu SY. Optimal direct output feedback of structural control. *Journal of Engineering Mechanics*, ASCE 1993; 2157–2173.
10. Lin CC, Chung LL, Sheu JF, Chu SY. Time delay effect and its solution for output feedback control of structures. *Earthquake Engineering and Structural Dynamics*, 1996; **25**: 547–559.
11. Chung LL, Wu LY, Jin TG. Acceleration feedback control of seismic structures. *Engineering Structures*, 1998; **20**: 62–74.
12. Yang JN, Akbarpour A, Ghaemmaghami P. Instantaneous optimal laws under seismic excitation. *Technical Report NCEER-87-0007*, National Center for Earthquake Engineering Research, Washington, DC, 10 June, 1987.
13. Chung LL, Wang YP, Tung CC. Instantaneous control of structures with time-delay considerations. *Engineering Structures*, 1997; **19**(6): 465–475.

